

**Measuring lepton flavor violation at LHC with a long-lived slepton in the coannihilation region**Satoru Kaneko,<sup>1,2,\*</sup> Joe Sato,<sup>3,†</sup> Takashi Shimomura,<sup>4,‡</sup> Oscar Vives,<sup>4,§</sup> and Masato Yamanaka<sup>3,||</sup><sup>1</sup>*Instituto Física Corpuscular - C.S.I.C./Universitat de València Campus de Paterna, Apt 22085, E46071, València, Spain*<sup>2</sup>*CFTP, Departamento de Física Instituto Superior Técnico, Avenida Rovisco Pais, 1 1049-001 Lisboa, Portugal*<sup>3</sup>*Department of Physics, Saitama University, Shimo-Okubo, Sakura-ku, Saitama, 338-8570, Japan*<sup>4</sup>*Departament de Física Teòrica and IFIC, Universitat de València - CSIC, E46100, Burjassot, València, Spain*

(Received 12 November 2008; published 19 December 2008)

When the mass difference between the lightest slepton, the next to lightest supersymmetric particle, and the lightest neutralino, the lightest supersymmetric particle, is smaller than the tau mass, the lifetime of the lightest slepton increases in many orders of magnitude with respect to typical lifetimes of other supersymmetric particles. These small mass differences are possible in the minimal supersymmetric standard model (MSSM) and, for instance, they correspond to the coannihilation region of the constrained MSSM for  $M_{1/2} \gtrsim 700$  GeV. In a general gravity-mediated MSSM, where the lightest supersymmetric particle is the neutralino, the lifetime of the lightest slepton is inversely proportional to the square of the intergenerational mixing in the slepton mass matrices. Such a long-lived slepton would produce a distinctive signature at LHC and a measurement of its lifetime would be relatively simple. Therefore, the long-lived slepton scenario offers an excellent opportunity to study lepton flavor violation at ATLAS and CMS detectors in the LHC and an improvement of the leptonic mass insertion bounds by more than 5 orders of magnitude would be possible.

DOI: [10.1103/PhysRevD.78.116013](https://doi.org/10.1103/PhysRevD.78.116013)

PACS numbers: 11.30.Hv, 12.60.Jv, 14.80.Ly

**I. INTRODUCTION**

Cosmological observations have confirmed the existence of the nonbaryonic dark matter. The observed dark matter (DM) relic abundance is  $\Omega_{\text{DM}} h^2 \simeq 0.11$  and points to the existence of a stable and weakly interacting particle with a mass  $m = 100\text{--}1000$  GeV. In supersymmetric (SUSY) models with conserved  $R$  parity, the lightest supersymmetric particle (LSP), usually the lightest neutralino, is stable and it is a perfect candidate for the dark matter. In fact, although the dark matter abundance in an arbitrary point of the SUSY parameter space is usually too large and only in regions where the LSP abundance is lowered effectively by annihilation, the observed abundance can be reached. One of the best mechanisms to lower the dark matter abundance is the so-called coannihilation [1]. In the coannihilation region, the next to lightest supersymmetric particle (NLSP) has a mass nearly degenerate to the LSP. Then the NLSP and the LSP decouple from thermal bath almost simultaneously and the LSP annihilates efficiently through collisions with the NLSP. The degeneracy required for the coannihilation to occur is generally  $\delta m/m_{\text{LSP}} < a$  few percent, where  $\delta m = m_{\text{NLSP}} - m_{\text{LSP}}$ . Numerically, this mass difference at a fixed  $\tan\beta$  value ranges from  $\delta m \simeq 10$  GeV for low  $M_{1/2}$  to practically zero at large  $M_{1/2}$ , where  $M_{1/2}$  is the universal gaugino mass.

Furthermore, it was pointed out in [2–4] that if staus are the NLSP and its mass difference with the LSP is less than the tau mass, they destroy  ${}^7\text{Li}/{}^7\text{Be}$  nucleus through the internal conversion. With this small mass difference, staus become long lived, they survive until big-bang nucleosynthesis starts and form bound states with a nucleus. The stau-nucleus bound states decay immediately by virtual exchange of the hadronic current. In this way, it was shown that the relic abundance of the light elements is lowered effectively and the discrepancy between the observed value of  ${}^7\text{Li}/{}^7\text{Be}$  abundance [5,6] and the predicted value from the standard big-bang nucleosynthesis [7] with WMAP data [8,9] can be solved. Thus, a scenario with stau NLSP and neutralino LSP with  $\delta m \leq m_\tau$  could explain the relic abundance of the light elements as well as the abundance of the dark matter. At this point, we could ask whether this small mass difference is really possible in the parameter space of the minimal supersymmetric standard model (MSSM) or even the constrained MSSM (CMSSM) consistently with dark matter constraints. As we will show below,  $\delta m \leq m_\tau$  and even smaller values are possible in the CMSSM. As shown in [2], if the mass difference,  $\delta m$ , between neutralino and stau is less than the tau mass, the two-body decay is forbidden and the lifetime of stau increases by more than 10 orders of magnitude.

Strictly speaking, the previous discussion is correct only in the framework of the MSSM without intergenerational mixing in the slepton sector, as could be, for instance, the CMSSM defined at the grand unified theory (GUT) scale without right-handed neutrinos, or neutrino Yukawa couplings. In this case, the NLSP is only a combination of left- and right-handed staus. However, there is no doubt that, in

\*satoru@cftp.ist.utl.pt

†joe@phy.saitama-u.ac.jp

‡takashi.shimomura@uv.es

§oscar.vives@uv.es

||masa@krishna.th.phy.saitama-u.ac.jp

a general MSSM we naturally expect some degree of inter-generational mixing in the sfermion sector. Even starting from a completely universal MSSM at  $M_{\text{GUT}}$  in the presence of neutrino Yukawa couplings, a small mixing between different sleptons is generated by renormalization group equations. Moreover, there is no fundamental reason to restrict the flavor structures to the Yukawa couplings and keep the soft mass matrices universal. In fact, we would expect the same mechanism responsible for the origin of flavor to generate some flavor mixing in the sfermion sector. As an example, we have flavor symmetries [10,11] where we expect similar flavor structures in the Yukawas and the scalar mass matrices. Therefore, in general, we expect that the lightest slepton,  $\tilde{l}_1$ , is not a pure stau, but there is some mixing with smuon and selectron. In the presence of this small intergenerational mixing, even with  $\delta m \leq m_\tau$ , other two-body decay channels like  $\tilde{l}_1 \rightarrow \tilde{\chi}_1^0 + e(\mu)$ , are still open [2]. In this case, given that the flavor conserving two-body decay channel is closed, the slepton lifetime will have a very good sensitivity to small lepton flavor violation (LFV) parameters. The lifetime will be inversely proportional to the sfermion mixing until two-body decay width becomes comparable to three- or four-body decay widths. Thus, it is worthwhile to study the lifetime of the sleptons in the small  $\delta m$  case to obtain information on LFV parameters. Several papers have studied in the past the possibility of measuring LFV at colliders [12–19]. However, in these papers the LFV decays are always subdominant with small branching ratios and is never possible to reach the level of sensitivity we reach in our scenario. Only Ref. [16] considers LFV in  $e^+e^-$  colliders through the slepton production in a long-lived stau scenario in a gauge-mediated model and as in the other works they are not sensitive either to the presence of small lepton flavor violation that we consider here.

Long-lived charged particles are very interesting since they provide a clear experimental signature at the LHC [20–22]. In Ref. [23], they conclude that even if the lifetime of the decaying particle is much longer than the size of the detector, some decays always take place inside the detector and it is possible to measure lifetimes as long as  $10^{-5}$ – $10^{-3}$  sec in a particular gauge mediation scenario.

In this paper, we study LFV in the coannihilation region of the MSSM with neutralino LSP and slepton NLSP with a mass difference  $\delta m \leq m_\tau$ . The paper is organized as follows. In Sec. II, we study the case of the MSSM without flavor mixing in the slepton sector. Here, we show that a sizable part of the coannihilation region at large  $M_{1/2}$  has the  $\delta m \leq m_\tau$  region satisfying all the experimental constraints and we calculate the lifetime of the NLSP. Then, in Sec. III, we introduce a source of lepton flavor violation in the slepton mass matrices and we recalculate the lifetimes in terms of the LFV parameters. In Sec. IV, we discuss the expected phenomenology of this scenario at the LHC and how LHC data could be used to measure small LFV

parameters. Finally, in Sec. V, we present our summary and discussion.

## II. LONG-LIVED STAU IN MSSM

We start our analysis looking for allowed regions in the CMSSM parameter space where the mass difference,  $\delta m$ , between the lightest neutralino mass,  $m_{\tilde{\chi}_1^0}$ , and the lighter stau mass,  $m_{\tilde{\tau}_1}$ , is smaller than tau mass,  $m_\tau$ . In this section, we consider the case of a constrained MSSM defined at the GUT scale without neutrino Yukawa couplings. Thus, in this case,  $\tilde{\tau}_1$  is equal to a combination of the right- and left-handed stau and no LFV effects are present. The CMSSM is parametrized by four parameters and a sign,

$$\{M_{1/2}, m_0, A_0, \tan\beta, \text{sign}(\mu)\}, \quad (1)$$

where the first three parameters are the universal gaugino and scalar masses, and the universal trilinear couplings at the GUT scale,  $\tan\beta$  is the ratio of vacuum expectation values of two Higgses, and  $\mu$  is the Higgs mass parameter in the superpotential. In our numerical analysis, we use SPheno [24] to obtain the parameters and mass spectrum at electroweak scale and use micrOMEGAS [25] to calculate relic dark matter abundance.

First, we list the experimental constraints that we have used in our analysis. The main constraint, apart from direct limits on SUSY masses, comes from the relic density of the dark matter abundance as reported by the WMAP Collaboration in Ref. [9]:

$$\Omega_{\text{DM}} h^2 = 0.1099 \pm 0.0062. \quad (2)$$

In this paper, we use more conservative range,

$$0.08 < \Omega_{\text{DM}} h^2 < 0.14, \quad (3)$$

but the results would remain basically unchained with a smaller range.

A second constraint comes from the anomalous magnetic moment of the muon,  $a_\mu = (g - 2)_\mu/2$ , that has been measured precisely in the experiments at BNL. The final experimental result [26] is

$$a_\mu^{(\text{exp})} = (11\,659\,208.0 \pm 6.3) \times 10^{-10}, \quad (4)$$

and the standard model (SM) prediction is

$$a_\mu^{(\text{SM})} = (11\,659\,180.5 \pm 5.6) \times 10^{-10}. \quad (5)$$

Therefore, the difference between the experiment and the standard model prediction is given [27] as

$$\Delta a_\mu = a_\mu^{(\text{exp})} - a_\mu^{(\text{SM})} = (27.5 \pm 8.4) \times 10^{-10} \quad (6)$$

which corresponds to a difference of 3.3 standard deviations. These results seem to require a positive and sizable SUSY contribution to  $a_\mu$ , although it is still not conclusive. In the following, in all our plots we will show the regions favored by measurement of  $a_\mu$  at a given confidence level,

but we will not use it as a constraint to exclude the different points. The bound on  $\text{Br}(b \rightarrow s\gamma)$  is also taken into account, but as we will see, in the region of small  $\delta m$  and correct dark matter abundance,  $M_{1/2} \geq 700$  GeV. Therefore the numerical prediction we obtained for  $\text{Br}(b \rightarrow s\gamma)$  is always very close to the SM predictions.

In Fig. 1, we show the allowed parameter regions in the  $M_{1/2}-m_0$  plane for  $\tan\beta = 10, 30, 45$  and  $A_0 = 600$  GeV. The sign of  $\mu$  is taken to be positive in all figures as required by the  $b \rightarrow s\gamma$  and  $a_\mu$  constraints. In these figures, the solid lines indicate the different confidence level regions for the  $a_\mu$  constraint. The yellow (light) narrow band is the region with correct dark matter abundance corresponding to the coannihilation region and with  $\delta m > m_\tau$ . The red (dark) band in the coannihilation region represents the points with correct dark matter abundance and  $\delta m < m_\tau$ . The green regions are not consistent with the dark matter abundance, Eq. (3), while the white area is the stau LSP region and therefore is excluded. Note that in models where the observed dark matter abundance is accounted for other dark matter components besides the neutralino, the small  $\delta m$  region could be extended to the green regions below the yellow band. Notice that choosing

a positive and large  $A_0 (\simeq 3m_0)$ , the renormalization group evolved value  $A(M_W)$  is reduced with respect to the cases of zero or negative  $A_0$ . Therefore the left-right entry in the stau mass matrix,  $A - \mu \tan\beta$ , is also reduced. Then the region of neutralino LSP, for a fixed value of the neutralino mass,  $m_{\tilde{\chi}_1^0} (\simeq 0.4M_{1/2})$ , corresponds to smaller values of  $m_0$  for positive  $A_0$  than for zero or negative  $A_0$ . Therefore this implies slightly lighter spectrum and larger contributions to  $a_\mu$ . Anyway, the main features of the plots are maintained for different values of  $A_0$  with only this slight increase in the masses. From these plots we can see that the interesting region of correct value of dark matter relic abundance and  $\delta m < m_\tau$  corresponds always to relatively large values of  $M_{1/2}$ . This is due to the fact that the coannihilation cross section decreases at larger SUSY masses [28] and for sufficiently large  $M_{1/2}$  the cross section is too small to produce a correct dark matter abundance, even for  $m_{\tilde{\tau}_1} \simeq m_{\tilde{\chi}_1^0}$ .

Comparing the different  $\tan\beta$  values, we can see that at low  $\tan\beta$  the long-lived stau region corresponds to smaller values of  $m_0 \sim (120, 200)$  GeV, although it can only reach the  $a_\mu$  favored region at  $3\sigma$ . For  $\tan\beta = 30$ , the long-lived stau region corresponds to similar values of  $M_{1/2}$ , but the

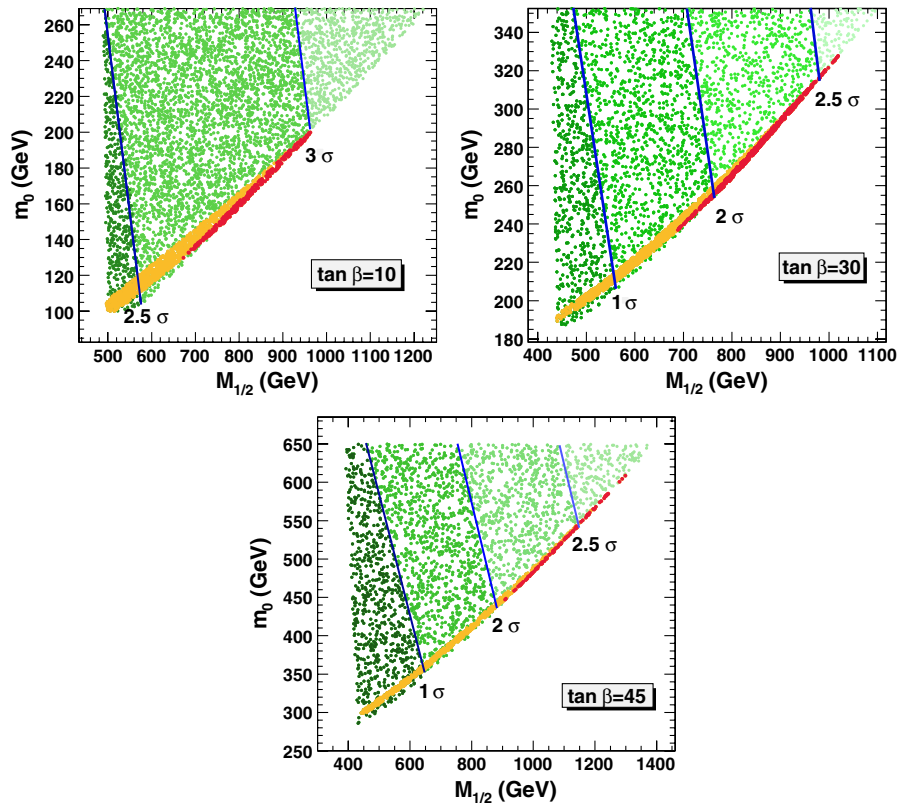


FIG. 1 (color online). The allowed parameter regions in  $M_{1/2} - m_0$  plane fixing  $A_0 = 600$  GeV.  $\tan\beta$  is varied 10, 30, 45 shown in each figure. The red (dark) narrow band is the consistent region with dark matter abundance and  $\delta m < m_\tau$  and the yellow (light) narrow band is that with  $\delta m > m_\tau$ . The green regions are inconsistent with the dark matter abundance, and the white area is stau LSP region and excluded. The favored regions of the muon anomalous magnetic moment at  $1\sigma$ ,  $2\sigma$ ,  $2.5\sigma$ , and  $3\sigma$  confidence level are indicated by solid lines.

TABLE I. Approximate mass ranges for points in the coannihilation region with  $m_{\tilde{\tau}_1} - m_{\tilde{\chi}_1^0} \leq 1.77$  GeV and within the  $2\sigma$  allowed region for  $a_\mu$  for  $\tan\beta = 30$ ,  $A_0 = 600$  GeV. These points correspond to  $m_0 \in (230, 250)$  GeV and  $M_{1/2} \in (700, 800)$  GeV.  $\tilde{u}$ ,  $\tilde{d}$  and  $\tilde{e}$ ,  $\tilde{\nu}_1$  denote the first two generation up-type, down-type squarks, and sleptons and sneutrinos.

	Mass (GeV)		Mass (GeV)
$\tilde{\chi}_1^0$	290–320	$\tilde{\chi}_2^0$	540–600
$\tilde{\chi}_3^0$	750–820	$\tilde{\chi}_4^0$	770–830
$\tilde{\chi}_1^\pm$	540–600	$\tilde{\chi}_2^\pm$	770–830
$\tilde{g}$	1540–1680		
$\tilde{t}_1$	1150–1260	$\tilde{t}_2$	1330–1460
$\tilde{b}_1$	1300–1420	$\tilde{b}_2$	1340–1460
$\tilde{u}_R$	1370–1500	$\tilde{u}_L$	1430–1560
$\tilde{d}_R$	1370–1500	$\tilde{d}_L$	1430–1560
$\tilde{\tau}_1$	290–320	$\tilde{\tau}_2$	510–560
$\tilde{e}_R$	350–385	$\tilde{e}_L$	520–570
$\tilde{\nu}_1$	500–550	$\tilde{\nu}_3$	510–560
$h$	116–118	$H$	800–900
$A$	800–900	$H^\pm$	800–900

required values of  $m_0$  are nearly a factor of 2 larger. However, in this case the larger value of  $\tan\beta$  allows this region to reach the  $a_\mu$  favored region at the  $2\sigma$  level. At  $\tan\beta = 45$  the long-lived stau region corresponds to larger values of both  $M_{1/2}$  and  $m_0$  and it can only reach the  $a_\mu$  favored region at  $2.5\sigma$ . This behavior of the allowed regions can be understood as follows. Since the SUSY contribution to  $a_\mu$  is proportional to  $\tan\beta/m_{\tilde{\chi}_1^0}^2$ , it is small when  $\tan\beta = 10$ . But it is also suppressed at  $\tan\beta > 30$  because the mass of the neutralino becomes heavier for large  $\tan\beta$ . With fixed  $A_0$ , the neutralino mass is determined mainly by  $M_{1/2}$  and the increase of the neutralino mass according to the increase of  $\tan\beta$  is seen in Fig. 1.

In these figures, we have seen that  $\delta m < m_\tau$  is possible in the CMSSM at  $M_{1/2} \gtrsim 700$  GeV and  $m_0 \gtrsim 200$  GeV. For these parameters, the resulting SUSY mass spectrum is relatively heavy. In Table I, we show the SUSY mass spectrum for the interesting region at  $\tan\beta = 30$  and  $A_0 =$

600 GeV. As can be seen in this table, masses of the lightest neutralino and the lightest slepton are around 300 GeV. It is important to emphasize that the lightest neutralino is mainly bino and the second lightest neutralino is wino with a small admixture of Higgsino. The second lightest neutralino and the lightest chargino have masses  $\sim 550$  GeV. The remaining two neutralino states and the heavier chargino are mainly Higgsinos with masses  $\sim 800$  GeV. The right-handed sleptons are in the range 300–390 GeV and the left-handed sleptons have masses of 510–570 GeV. The squarks are in the range 1150–1560 GeV while gluinos are heavier than the squarks and about 1540–1680 GeV. Finally, the lightest Higgs has a mass of  $\sim 116$  GeV and the heavier Higgses have masses of 800–900 GeV. With this spectrum, the lightest slepton is produced through decays of the heavier neutralinos, the charginos, and the left-handed squarks in longer decay chains. Neutralinos and charginos are produced via decays of squarks and gluinos. Although squarks and gluinos are relatively heavy, they are still in kinematical reach and can be produced at LHC experiments.

The decay rates of the NLSP stau into two, three, and four bodies shown in Fig. 2 are approximately given by

$$\Gamma_{2\text{-body}} = \frac{g_2^2 \tan^2 \theta_W}{2\pi m_{\tilde{\tau}_1}} \delta m \sqrt{(\delta m)^2 - m_\tau^2}, \quad (7)$$

$$\Gamma_{3\text{-body}} = \frac{g_2^2 G_F^2 f_\pi^2 \cos^2 \theta_c \tan^2 \theta_W}{30(2\pi)^3 m_{\tilde{\tau}_1} m_\tau^2} \delta m ((\delta m)^2 - m_\pi^2)^{5/2}, \quad (8)$$

$$\Gamma_{4\text{-body}} = \frac{2}{3} \frac{g_2^2 G_F^2 \tan^2 \theta_W}{5^3 (2\pi)^5 m_{\tilde{\tau}_1} m_\tau^2} \delta m ((\delta m)^2 - m_l^2)^{5/2} \times (2(\delta m)^2 - 23m_l^2), \quad (9)$$

where the notations and the relevant Lagrangian, the exact decay rates are given in the Appendix. Notice that when  $\delta m \gtrsim m_\tau$  the two-body decay is open and the lifetime of the stau,  $\tau_{\tilde{\tau}_1}$ , is  $\lesssim 10^{-22}$  sec. However, for  $\delta m \lesssim m_\tau$  this decay is closed and the three or four-body decays are

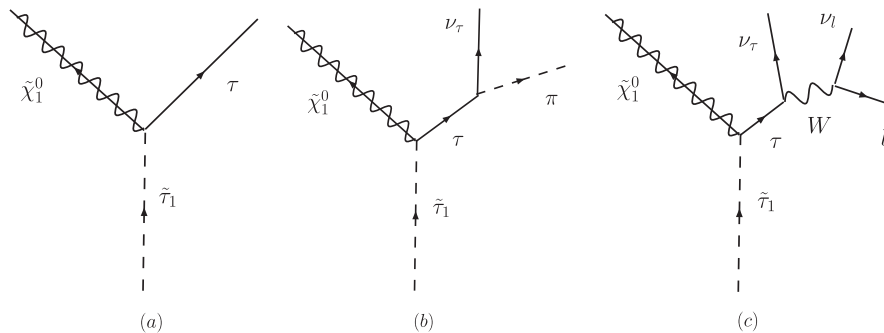


FIG. 2. Feynman diagrams of stau decay: (a) two-body decay, (b) three-body decay, (c) four-body decay.  $l$  denotes the charged leptons.

suppressed at least by an additional  $(\delta m)^4 G_F^2 (f_\pi/m_\tau)^2 1/(30(2\pi)^2) \simeq 10^{-13}$  with  $\delta m \sim 2$  GeV. Therefore the stau becomes long lived and the phenomenology of the MSSM changes dramatically [29].

### III. LFV AND LONG-LIVED SLEPTON

In the previous section, we have seen that  $\delta m \leq m_\tau$  is indeed possible in the framework of a CMSSM without LFV couplings. The lifetime of the NLSP stau in this scenario is increased by many orders of magnitude. However, a complete absence of flavor mixing in the sfermion mass matrices is not expected in realistic models. In general, we would expect a certain degree of intergenerational mixing to be present in the slepton sector. Once a new source of LFVs is introduced, the NLSP two-body decay channels into electron and/or muon can open again. In this case, the lifetime is inversely proportional to the square of the mixing of selectron and smuon with stau and therefore the measurement of the lifetime shows a strong sensitivity to LFV parameters. In this section, we show the dependence of the lifetime of the lightest slepton on the right-handed and the left-handed slepton mixings. All the numerical results of lifetimes and figures presented below are calculated using the exact formula in the Appendix.

To understand the dependence of lifetimes on LFV parameters, it is convenient to introduce the so-called mass insertions (MI),  $(\delta_{RR/LL}^e)_{\alpha\beta}$ , defined

$$(\delta_{RR/LL}^e)_{\alpha\beta} = \frac{\Delta M_{RR/LL\alpha\beta}^{e2}}{M_{R/L\alpha}^e M_{R/L\beta}^e}, \quad (10)$$

where  $\alpha, \beta$  denote the lepton flavors.  $M_{R/L\alpha}^e$  and  $M_{R/L\beta}^e$  are diagonal elements of the slepton mass matrix, and  $\Delta M_{RR/LL\alpha\beta}^e$  are off diagonal elements we introduced. In terms of these mass insertions, the two-body decay rate is approximately given by

$$\Gamma_{2\text{-body}} = \frac{g_2^2}{2\pi m_{\tilde{\tau}_1}} (\delta m)^2 (|g_{1\alpha 1}^L|^2 + |g_{1\alpha 1}^R|^2), \quad (11)$$

where  $\alpha = e, \mu$ .  $g_{1\alpha 1}^{L,R}$  can be approximated in the mass insertion as shown in Fig. 3. In the case of right-handed slepton mixing, we have,

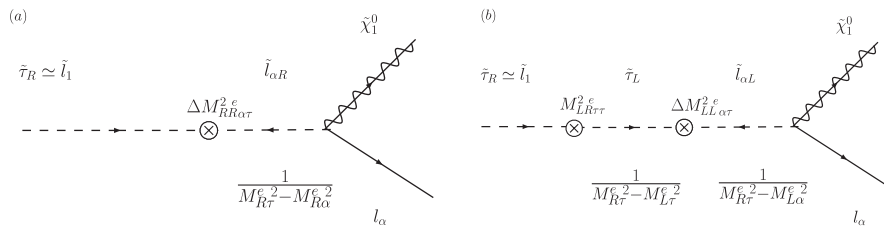


FIG. 3. MI Feynman diagrams of two-body slepton decay: The diagram on the left side depicts two-body decay in the presence of  $\delta_{RR}^e$  and the diagram on the right side in the presence of  $\delta_{LL}^e$ . The circle-crosses represent mass insertions for flavor and left-right chirality changes. Propagators for intermediate states are shown below the corresponding scalar lines.

$$g_{1\alpha 1}^L \simeq 0, \quad g_{1\alpha 1}^R \simeq \tan\theta_W \frac{M_{R\tau}^e M_{R\alpha}^e}{M_{R\tau}^{e2} - M_{R\alpha}^{e2}} (\delta_{RR}^e)_{\alpha\tau}, \quad (12)$$

while in the left-handed slepton mixing case, these couplings are given

$$g_{1\alpha 1}^L \simeq \frac{1}{2} \tan\theta_W \frac{m_\tau (A_0 - \mu \tan\beta)}{M_{R\tau}^{e2} - M_{L\tau}^{e2}} \frac{M_{L\alpha}^e M_{R\tau}^e}{M_{R\tau}^{e2} - M_{L\alpha}^{e2}} (\delta_{LL}^e)_{\alpha\tau},$$

$$g_{1\alpha 1}^R \simeq 0. \quad (13)$$

To analyze the effects of the presence of a nonvanishing leptonic mass insertion on the NLSP lifetime we choose four points with different mass differences as shown in Table II. In Fig. 4(a), we show the lifetime of the lightest slepton,  $\tau_{\tilde{l}_1}$ , as a function of  $(\delta_{RR}^e)_{e\tau}$ , encoding the right-handed selectron-stau mixing, that we vary from  $10^{-10}$  to  $10^{-2}$ . We can see that the lifetime for  $\delta m > m_\tau$  (case A in Table II) does not change, because the decay of slepton to tau and neutralino is always the dominant decay mode and the lifetime is insensitive to  $\delta_{RR}^e (\leq 10^{-2})$ . On the other hand, for  $\delta m < m_\tau$ , the lifetime grows more than 13 orders of magnitude in the limit  $(\delta_{RR}^e)_{e\tau} \rightarrow 0$ , where the three- or four-body decay processes are dominant. Then, the two-body decay into  $\tau$  and  $\tilde{\chi}_1^0$  is forbidden but those into  $e$  (or  $\mu$  for  $(\delta_{RR}^e)_{\mu\tau} \neq 0$ ) and  $\tilde{\chi}_1^0$  are allowed through LFV couplings. The lifetime decreases proportionally to  $|(\delta_{RR}^e)_{e\tau}|^{-2}$  when the two-body decay dominates total decay width. For values of  $\delta^e > 10^{-2}$  the mass of the lightest slepton would be substantially changed by this large off diagonal entry and this would reduce the mass difference changing the simple  $|(\delta_{RR}^e)_{e\tau}|^{-2}$  proportionality. This can be seen as an increase of the lifetime in case D at  $(\delta_{RR}^e)_{\mu\tau} \simeq 10^{-2}$  in Fig. 4(b). Although  $\delta_{RR}^e > 10^{-2}$  is still allowed by experiments as shown in Table III, we concentrate our discussion on  $\delta_{RR}^e \leq 10^{-2}$  to show the sensitivity of this process to small  $\delta_{RR}^e$ s. In fact, from these figures we can see that the lifetime indeed has very good sensitivity to small  $\delta^e$ s in this scenario. The present bounds on the different mass insertions for the spectrum considered here are shown in Table III. Comparing this table with the figures, we can see that the sensitivity obtained in the measurement of the NLSP lifetime can not be reached by indirect experiments as  $\tau \rightarrow \mu\gamma$  and  $\tau \rightarrow e\gamma$ , etc. Plot (b) in Fig. 4 corresponds to the right-handed smuon-stau mix-

TABLE II. Table of the mass difference and the lightest slepton, neutralino masses.  $m_0$ ,  $A_0$ , and  $\tan\beta$  are fixed to 260 GeV, 600 GeV, and 30, respectively. The values of neutralino abundance and  $a_\mu$  are shown for the reference.

No.	$\delta m$ (GeV)	$m_{\tilde{\chi}_1^0}$ (GeV)	$m_{\tilde{l}_1}$ (GeV)	$\Omega_{\tilde{\chi}_1^0} h^2$	$a_\mu (\times 10^{-10})$
A	2.227	323.1549	325.3817	0.110	10.32
B	1.650	325.5601	326.2147	0.102	10.25
C	0.407	327.6294	328.0365	0.085	10.09
D	0.092	328.4060	328.4981	0.081	10.06

ing,  $(\delta_{RR}^e)_{\mu\tau}$ . The lifetime is constant for  $\delta m = 0.09$  GeV in small  $(\delta_{RR}^e)_{\mu\tau}$  as the two-body decay in muon is still forbidden. For larger  $\delta m$ , we observe again the same dependence on  $(\delta_{RR}^e)_{\mu\tau}$ .

Figures 5(a) and 5(b) show the lifetime of the lightest slepton as a function of  $(\delta_{LL}^e)_{e\tau}$  and  $(\delta_{LL}^e)_{\mu\tau}$ , respectively. The different curves correspond to the same mass differences used in Fig. 4. The dependence on these mass insertions in these figures is completely analogous to the behavior observed in Fig. 4. In fact, both figures would be

identical if we replace  $(\delta_{LL}^e)$  by  $10 \times (\delta_{RR}^e)$ . This is due to the fact that in this case, the lightest slepton decays into the electron or the muon through the left-handed stau component. The mixing of right- and left-handed staus, Eq. (13), is proportional to  $m_\tau(A_0 - \mu \tan\beta)/(M_{R\tau}^2 - M_{L\tau}^2)$ . In the region of parameter space, we are considering this factor is approximately 0.1. Thus, we can see that, also in the case of  $(\delta_{LL}^e)$ , the lifetime is sensitive to the presence of very small lepton flavor violating couplings and therefore to the presence of mass insertions orders of magnitude smaller than the present bounds.

At this point, we have seen that even very small values of the mass insertions are observable if nature happens to choose the coannihilation region in the MSSM for relatively large values of  $M_{1/2}$ . Now, we can ask what is the expected size for these  $\delta^e$  in different models. The first example, always present if we introduce right-handed neutrinos in the theory, is the supersymmetric seesaw mechanism. In this model we simply introduce right-handed neutrinos with Yukawa couplings to the Higgs and lepton doublets [34–48]. These Yukawa couplings induce some nonvanishing off diagonal entries in the left-handed slep-

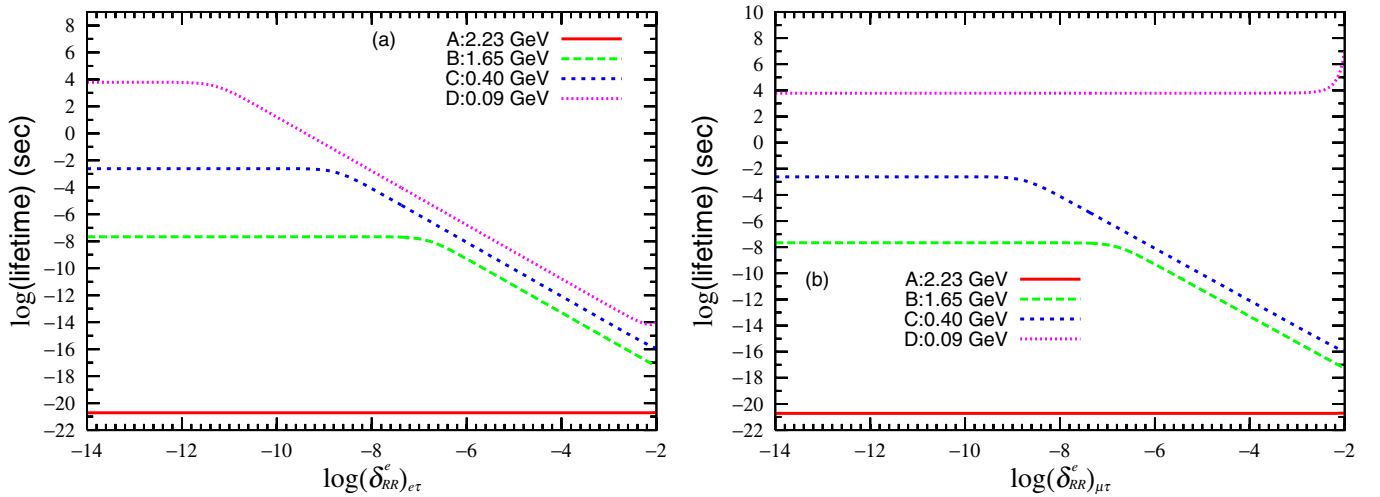


FIG. 4 (color online). The lifetime of the lightest slepton as a function of  $\delta_{RR}^e$ . The left panel, (a), is the lifetime of the lightest slepton with the right-handed selectron and stau mixing, and the right panel, (b), is the one with the right-handed smuon and stau mixing. In both panels, the solid (red), dashed (green), dotted (blue), dotted-dashed (pink) lines correspond to  $\delta m = 2.23(A)$ , 1.65(B), 0.41(C), 0.09(D) GeV, respectively.  $m_0 = 260$  GeV,  $A_0 = 600$  GeV, and  $M_{1/2}$  are varied.  $0.08 < \Omega_{\tilde{\chi}_1^0} h^2 < 0.14$  is required. These lifetimes are calculated with the exact formulas in the Appendix.

TABLE III. Mass insertion bounds for a typical point in the long-lived stau coannihilation region with  $m_0 = 267$  GeV,  $M_{1/2} = 750$  GeV,  $A_0 = 600$  GeV, and different values of  $\tan\beta$  [31–33]. These bounds are obtained from the experimental limits ( $\text{BR}(\mu \rightarrow e\gamma) < 1.2 \times 10^{-11}$ ,  $\text{BR}(\tau \rightarrow e\gamma) < 1.1 \times 10^{-7}$ ,  $\text{BR}(\tau \rightarrow \mu\gamma) < 0.45 \times 10^{-7}$ ).

	$\tan\beta = 10$			$\tan\beta = 30$			$\tan\beta = 45$		
	$\delta_{e\mu}^e$	$\delta_{e\tau}^e$	$\delta_{\mu\tau}^e$	$\delta_{e\mu}^e$	$\delta_{e\tau}^e$	$\delta_{\mu\tau}^e$	$\delta_{e\mu}^e$	$\delta_{e\tau}^e$	$\delta_{\mu\tau}^e$
LL	0.0014	0.33	0.21	0.00047	0.10	0.068	0.00030	0.067	0.043
RR	0.0060	1.7	1.1	0.0019	0.44	0.29	0.0012	0.28	0.18

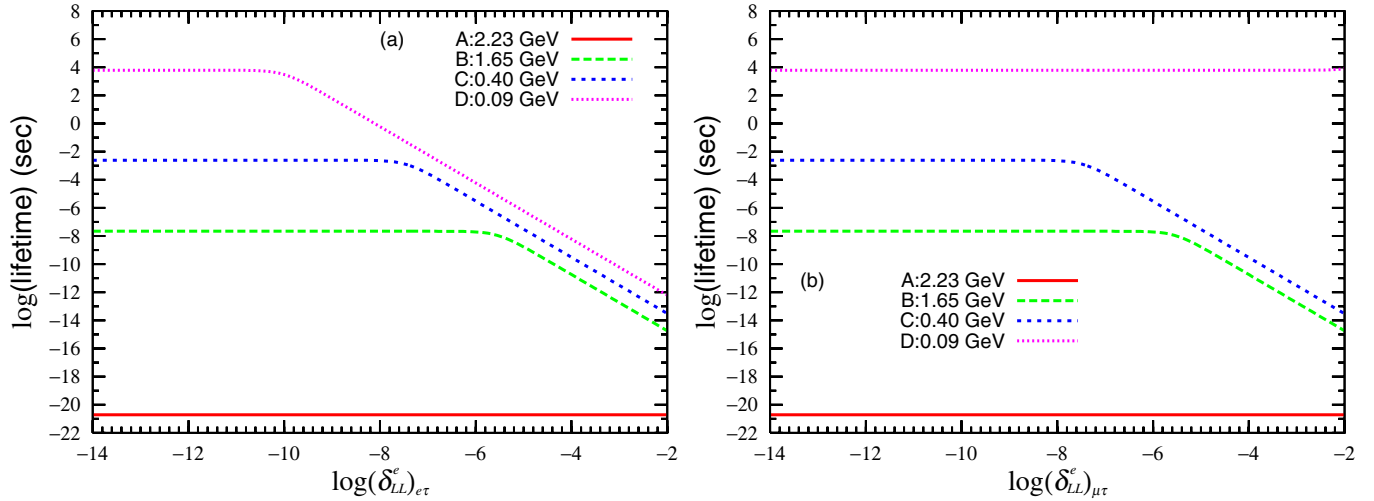


FIG. 5 (color online). The lifetime of the lightest slepton as a function of  $\delta_{LL}^e$ . The lines and the parameters are the same as Fig. 4.

ton mass matrices through the renormalization group evolution (RGE) from  $M_{\text{GUT}}$  to  $M_W$ . The value of the induced  $\delta^e$ s depends on the considered neutrino Yukawa couplings and this is model dependent. Nevertheless, it is usually assumed that the neutrino Yukawa couplings are related to the up-quark Yukawa couplings, as happens in  $SO(10)$  GUT models. Then, we have two main possibilities for this Yukawa matrix, it can have large (Maki-Nakagawa-Sakata-like) or small (Cabibbo-Kobayashi-Maskawa-like) mixings [43]. In the case of large mixings with  $y_3 \approx y_1 \approx 1$ , where  $y_3$  and  $y_1$  are the largest eigenvalues in the neutrino and up-squark Yukawa matrices,  $(\delta_{LL}^e)_{e\tau} \approx 0.1U_{e3}$ , with  $U_{e3} \leq 0.18$  still not measured in the Maki-Nakagawa-Sakata matrix, and  $(\delta_{LL}^e)_{\mu\tau} \approx 0.05$ . This mixing is very large and would predict a lifetime  $\leq 10^{-14}$  sec. Even in the case of small mixings (Cabibbo-Kobayashi-Maskawa-like), the induced deltas are still sizable,  $(\delta_{LL}^e)_{e\tau} \approx 0.0008$  and  $(\delta_{LL}^e)_{\mu\tau} \approx 0.004$ , corresponding to lifetimes,  $\tau_{\tilde{l}_1} \sim 10^{-10}$  to  $10^{-13}$  sec and  $\tau_{\tilde{l}_1} \sim 10^{-12}$  to  $10^{-14}$  sec, respectively. These RGE effects from the seesaw mechanism are always present in the model irrespective of the initial structure of the slepton mass matrices at the GUT scale. It is also possible that the slepton mass matrices have a nontrivial structure at  $M_{\text{GUT}}$  if the same mechanism that generates the flavor structure in the Yukawa couplings generates simultaneously a flavor structure in the soft terms. This is the case of flavor symmetries in SUSY [11,31,49–51]. As an example we take the  $SU(3)$  flavor symmetry [31,49]. Typical values of the deltas in this case are  $(\delta_{RR}^e)_{e\tau} \approx 0.001$ ,  $(\delta_{RR}^e)_{\mu\tau} \approx 0.02$ ,  $(\delta_{LL}^e)_{e\tau} \approx 0.0008$ , and  $(\delta_{LL}^e)_{\mu\tau} \approx 0.004$  and therefore expected lifetimes would be in the range  $10^{-10}$  to  $10^{-16}$  sec. Notice that this model predicts only moderate flavor changing couplings in the slepton mass matrices and values in other models are typically larger or the same order as this [11]. Nonvanishing off diagonal entries in the slepton mass matrices are also generated by  $SU(5)$  or  $SO(10)$  RGE

evolution from  $M_{\text{Planck}}$  to  $M_{\text{GUT}}$  [52–55], and similar sizes of  $\delta^e$ s are expected in these models.

#### IV. LHC PHENOMENOLOGY

In this section, we discuss the expected phenomenology at LHC experiments, focusing mainly on the ATLAS detector [56,57], of the long-lived slepton scenario. The lightest slepton is the NLSP, and therefore a large number of sleptons is expected to be produced via cascade decays of heavier SUSY particles. When the long-lived sleptons have lifetimes between  $10^{-5}$  and  $10^{-12}$  sec, we will have a chance to observe decays of the slepton inside the detector. The ATLAS detector, whose dimensions are 25 m in height and 44 m in length, consists of inner detector, calorimeter, and muon detector [56]. The inner detector surrounds the collision point and is contained within a cylindrical envelop of length  $\pm 3.51$  m and of radius 1.15 m. In the inner detector, the pixel detector, the semiconductor tracker (SCT) and the transition radiation tracker are installed to measure momenta and decay vertices of charged particles. The pixel detector is placed around the collision point and consists of three barrels at average radii of 5, 9, and 12 cm, and three disks on each side, between radii of 9 and 15 cm. The SCT surrounds the pixel detector and consists of four barrels at radii of 30, 37, 44, and 52 cm. The transition radiation tracker is installed on outside of the SCT. It covers radial range from 56 to 107 cm. Surrounding the inner detector, hadronic, and electromagnetic calorimeters are placed over 4 m radius and 8.4 m length. The calorimeters are surrounded by the muon spectrometer which covers the ATLAS detector. In the following, we show that, in the relevant region of SUSY parameter space, we can see decays of sleptons with the lifetime up to  $10^{-5}$  seconds within the ATLAS detector. Although we discuss only the ATLAS detector, analysis is similar to the CMS detector [58].

First, we estimate the number of lightest sleptons produced at LHC. In our scenario, the lightest slepton is mainly a right-handed stau and the lightest neutralino is mainly bino. The SUSY spectrum in the long-lived stau region that we consider is presented in Table I. This spectrum corresponds approximately to the post-WMAP SUSY benchmark point  $J'$  proposed in [59,60] with a slightly different  $\tan\beta$  value ( $\tan\beta = 35$  versus  $\tan\beta = 30$  in our case). Then, the right-handed staus are mainly produced via decays of first two generation left-handed squarks, (number in parenthesis corresponds to branching ratios in each decay [59,60])

$$\tilde{q}_L \rightarrow \tilde{\chi}_1^\pm + q(0.63), \quad (14)$$

$$\tilde{\chi}_1^\pm \rightarrow \tilde{l}_1 + \nu_\tau(0.64), \quad \tilde{\nu}_\tau + \tau(0.27), \quad (15)$$

$$\tilde{\nu}_\tau \rightarrow \tilde{l}_1 + W(0.82), \quad (16)$$

$$\tilde{q}_L \rightarrow \tilde{\chi}_2^0 + q(0.36), \quad (17)$$

$$\tilde{\chi}_2^0 \rightarrow \tilde{l}_1 + \tau(0.66), \quad \tilde{\nu}_\tau + \nu_\tau(0.25), \quad (18)$$

where  $q$ ,  $\tilde{\chi}_1^\pm$ , and  $\tilde{\chi}_2^0$  denote the SM quarks, the lighter charginos, and the second lightest neutralinos and  $\nu_\tau$ ,  $W$ , and  $\tilde{\nu}_\tau$  denote tau neutrino, weak boson, and tau sneutrino, respectively. The third generation squarks have many different decay chains. For example

$$\tilde{t}_{1,2} \rightarrow \tilde{\chi}_1^\pm + b, \quad (0.20, 0.25) \quad (19)$$

$$\tilde{\chi}_1^\pm \rightarrow \tilde{l}_1 + \nu_\tau, \quad (20)$$

$$\tilde{t}_{1,2} \rightarrow \tilde{\chi}_2^0 + t, \quad (0.10, 0.10) \quad (21)$$

$$\tilde{\chi}_2^0 \rightarrow \tilde{l}_1 + \nu_\tau, \quad (22)$$

$$\tilde{b}_{1,2} \rightarrow \tilde{\chi}_1^\pm + t, \quad (0.36, 0.12) \quad (23)$$

$$\tilde{\chi}_1^\pm \rightarrow \tilde{l}_1 + \nu_\tau, \quad (24)$$

$$\tilde{b}_{1,2} \rightarrow \tilde{\chi}_2^0 + b, \quad (0.20, 0.10) \quad (25)$$

$$\tilde{\chi}_2^0 \rightarrow \tilde{l}_1 + \nu_\tau. \quad (26)$$

Total branching ratios for  $\tilde{l}_1$  production are 0.86 in  $\tilde{q}_L$  decay, 0.72/0.90 for  $\tilde{t}_1/\tilde{t}_2$ , and 0.87/0.67 for  $\tilde{b}_1/\tilde{b}_2$  at  $\tan\beta = 35$  [59–61]. On the other hand, the right-handed squarks, couple only to bino and Higgsino, having small Yukawa couplings, decay almost completely to the lightest neutralino and quarks. Therefore branching ratios of them into  $\tilde{l}_1$  and quarks/leptons are negligible. The total cross section of SUSY pair production in our scenario is given in [62,63],

$$\sigma_{\text{SUSY}} = 130 \text{ fb}. \quad (27)$$

When we assume the integrated luminosity,  $\mathcal{L}_{\text{int}} =$

$30 \text{ fb}^{-1}$ , which corresponds to three years of data taking with the luminosity,  $\mathcal{L} = 10^{33} \text{ cm}^{-2} \text{ s}^{-1}$ , the total number of SUSY pairs is 3900. Then, squarks are pair produced with equal probability for left- and right-handed squarks, thus, the number of lightest sleptons produced,  $N_{\tilde{l}_1}$ , is estimated as

$$N_{\tilde{l}_1} \simeq 4290. \quad (28)$$

Therefore we would have 4290 long-lived sleptons produced in ATLAS that could decay inside the detector depending on the lifetime. The decay probability is given

$$P_{\text{dec}}(l) = 1 - \exp\left(-\frac{l}{\beta\gamma c\tau_{\tilde{l}_1}}\right), \quad (29)$$

where  $\beta = v/c$  and  $\gamma = 1/\sqrt{1-\beta^2}$  with  $c$  the speed of the light,  $l$  is the distance between production and decay point. To obtain the expected number of decays, we need to know the distribution of  $\beta\gamma$ . This would require a full analysis with Monte Carlo simulation and it is beyond the scope of this paper. For the spectrum shown in Table I, the typical momentum of the lightest slepton is expected to be between 500 and 900 GeV.  $\beta\gamma$  corresponding to this range of momenta is

$$1.53 \lesssim \beta\gamma \lesssim 2.75, \quad (30)$$

hence we can assume  $\beta\gamma$  to be 2. Then, using Eq. (29), the expected number of the decays,  $N_{\text{dec}}$ , within a distance  $l$  is given

$$N_{\text{dec}}(l) = N_{\tilde{l}_1} P_{\text{dec}}(l) = N_{\tilde{l}_1} \left(1 - \exp\left(-\frac{l}{\beta\gamma c\tau_{\tilde{l}_1}}\right)\right). \quad (31)$$

In Table IV, we show the expected number of slepton decays in each detector, assuming the integrated luminosity,  $\mathcal{L}_{\text{int}} = 30 \text{ fb}^{-1}$  and  $\beta\gamma = 2$ . As can be seen, when the lifetime,  $\tau_{\tilde{l}_1}$ , is below  $10^{-9}$  sec, most of the sleptons decay inside the pixel detector. When  $\tau_{\tilde{l}_1} \sim 10^{-8}$  sec, almost half

TABLE IV. The expected number of slepton decay in the ATLAS detector. The length is the minimum (5 cm) and medium (50 cm) distance to the pixel detector and the maximum distance to the outer boundary of the detectors from the interaction point and corresponds to pixel detector (3.1 m), calorimeter (5.8 m), and muon spectrometer (25.0 m). The lifetime is varied from  $10^{-12}$  to  $10^{-5}$  sec. The number of sleptons produced at LHC assuming the integrated luminosity,  $\mathcal{L}_{\text{int}} = 30 \text{ fb}^{-1}$  is 4290 and  $\beta\gamma$  is fixed to 2.

	5 cm	50 cm	3.1 m	5.8 m	25.0 m
$10^{-5}$ sec	0.04	0.36	2.2	4.1	17.8
$10^{-6}$ sec	0.36	3.6	22.1	41.3	175.1
$10^{-7}$ sec	3.6	35.6	216.0	395.3	1461.9
$10^{-8}$ sec	35.6	343.0	1731.0	2658.3	4223.5
$10^{-9}$ sec	343.0	2425.6	4265.5	4289.7	4290.0
$10^{-10}$ sec	2425.6	4289.0	4290.0	4290.0	4290.0
$10^{-11}$ sec	4289.0	4290.0	4290.0	4290.0	4290.0
$10^{-12}$ sec	4290.0	4290.0	4290.0	4290.0	4290.0

of them decay inside the inner detector and nearly all of them decay within the detector. If  $\tau_{\tilde{l}_1}$  is between  $10^{-8}$  and  $10^{-6}$  sec, several hundreds of slepton decays occur inside the ATLAS detector. Almost all of them escape from the detector when  $\tau_{\tilde{l}_1} > 10^{-5}$  sec, although we expect of the order of 10 decays inside the detector for  $\tau_{\tilde{l}_1} \simeq 10^{-5}$  sec.

Sleptons with different lifetimes would give different signatures in the ATLAS detector. Depending on the lifetimes, sleptons would decay inside the detector or escape the detector as a stable heavy charged particle. For  $\tau_{\tilde{l}_1} < 10^{-11}$  sec, since almost all of the sleptons would decay before they reach the first layer of the pixel detector, we would not observe any heavy charged-particle track in the detector. In this case, it would be more difficult to identify the presence of long-lived sleptons at the ATLAS detector. This problem will be addressed in a future work [64]. For  $\tau_{\tilde{l}_1} \sim 10^{-10}$  to  $10^{-9}$  sec, almost all the sleptons would decay inside the pixel detector and leave a charged track with a kink. Then, a different charged particle would cross the outer detectors and a corresponding track and/or hit would be seen in each detector. Thus, by combining with signals in the outer detectors, we could identify whether the outgoing charged particle is an electron or muon. Then, if we can fix the mass difference between the lightest slepton and neutralino, we can determine the value of the mass insertion parameters from Figs. 4 and 5. In the case of the right-handed slepton mixing case, lifetimes between  $10^{-10}$  and  $10^{-8}$  sec would correspond to  $(\delta_{RR}^e)_{e\tau}$  between  $10^{-7}$  and  $10^{-4}$  with the mass difference,  $m_e < \delta m < m_\tau$ , and  $(\delta_{RR}^e)_{\mu\tau}$  between  $10^{-7}$  and  $10^{-5}$  with  $m_\mu < \delta m < m_\tau$ . Similarly, in the case of left-handed slepton mixing, the same lifetimes would correspond to  $(\delta_{LL}^e)_{e\tau}$  between  $4 \times 10^{-6}$  and  $10^{-3}$  with  $m_e < \delta m < m_\tau$ , and  $(\delta_{LL}^e)_{\mu\tau}$  between  $4 \times 10^{-6}$  and  $10^{-4}$  with  $m_\mu < \delta m < m_\tau$ . For  $\tau_{\tilde{l}_1} \sim 10^{-8}$  sec, about half of sleptons would decay inside the inner detector and the rest would decay inside the calorimeters and/or muon spectrometer. In this case, it would be important to determine whether the decay is LFV two-body decay or lepton flavor conserving three-body decay [64]. For lifetimes between  $10^{-7}$  and  $10^{-5}$  sec, very few sleptons would decay inside the pixel detector and most of them would escape the detector leaving a charged track with a corresponding hit in muon spectrometer. Even for particles escaping the detector, we could use a muon spectrometer to determine slepton mass and momentum as studied in [21,22]. For  $\tau_{\tilde{l}_1} \gtrsim 10^{-5}$  sec, very few sleptons would decay inside the ATLAS detector. In this case, we can put lower bound on the lifetime. Then, in a gravity-mediated scenario, this would correspond to a stringent upper bound on  $\delta^e$ s.

This scenario of long-lived slepton is in principle similar to the situation in gauge-mediated SUSY breaking scenario [23]. For similar lifetimes, more detailed analysis is needed to distinguish scenarios. However most of sleptons in

gauge-mediated SUSY breaking scenario would escape from the detector and we could see only a few events.

## V. SUMMARY

In this work, we have studied lepton flavor violation in a long-lived slepton scenario where the mass difference between the NLSP, the lightest slepton, and the LSP, the lightest neutralino, is smaller than the tau mass. With this small mass difference, the lifetime of the lightest slepton has a very good sensitivity to small lepton flavor violation parameters due to the more than 13 orders of magnitude suppression of the three-body decay rate with respect to the two-body decay rate.

We have shown that this small  $\delta m$  is possible even in the framework of the CMSSM. We selected the region in the CMSSM parameter space with  $\delta m < m_\tau$ , taking into account correct dark matter abundance and direct bounds on SUSY and Higgs masses and  $b \rightarrow s\gamma$  constraint. We have used the experimental results of the anomalous magnetic moment of the muon to indicate the favored regions at given confidence level. We have found that a small  $\delta m$  region consistent with all experimental constraints lies on a sizable part of the parameter space at  $M_{1/2} \gtrsim 700$  GeV,  $m_0 = 100$  to 600 GeV for different values of  $\tan\beta$ . We have also shown that the most favored region, which is consistent with  $a_\mu$  at  $2\sigma$ , corresponds to  $240 \lesssim m_0 \lesssim 260$  GeV and  $700 \lesssim M_{1/2} \lesssim 800$  GeV at  $\tan\beta = 35$ .

Then, we have analyzed the dependence of the lightest slepton lifetimes on different mass insertions,  $(\delta_{RR/LL}^e)_{e\tau,\mu\tau}$  for values of  $\delta m$  from 2.23 to 0.09 GeV. We found that the lifetimes are proportional to  $|\delta^e|^{-2}$  until three- or four-body decays become comparable. There is a difference of approximately a factor of 10 in the sensitivity of the lifetime on  $\delta_{RR}^e$  and  $\delta_{LL}^e$ . This is due to the different proportion of left-handed and right-handed staus in the lightest slepton. By comparing the values of the bounds on  $\delta^e$ s shown in Table III, we can see that, in this scenario, the lifetimes are sensitive to much smaller values of these  $\delta^e$ s, even to future sensitivities of proposed experiments.

Finally, we have discussed the expected phenomenology at LHC experiments, mainly concentrating on the ATLAS detector. We have estimated the number of slepton decays in the different detectors, assuming an integrated luminosity  $\mathcal{L}_{\text{int}} = 30 \text{ fb}^{-1}$  and  $\beta\gamma = 2$  (Table IV). We have seen that the ATLAS detector can observe lifetimes in the range of  $10^{-11}$  to  $10^{-6}$  sec, and these lifetimes would correspond to  $(\delta_{RR}^e)_{e\tau,\mu\tau}$  between  $10^{-7}$  and  $10^{-3}$  and  $(\delta_{LL}^e)_{e\tau,\mu\tau}$  between  $4 \times 10^{-6}$  and  $10^{-3}$ . Therefore we have shown that in the long-lived slepton scenario, the LHC offers a very good opportunity to study lepton flavor violation.

## ACKNOWLEDGMENTS

The authors, O.V. and T.S., would like to thank V. Mitsou for fruitful discussion on detection possibilities of

the long-lived slepton at the ATLAS detector, and J. Jones-Perez for numerical checks of bounds on mass insertions. S. K. was supported by European Commission Contracts No. MRTN-CT-2004-503369 and No. ILIAS/N6 WP1 RI I3-CT-2004-506222, and also Fundação para a Ciência e a Tecnologia (FCT, Portugal) through CFTP-FCT UNIT 777, which is partially funded through POCTI (FEDER). S. K. is an Experienced Researcher supported by the Marie Curie Research Training Network MRTN-CT-2006-035505. The work of J. S. was supported in part by the Grant-in-Aid for the Ministry of Education, Culture, Sports, Science, and Technology, Government of Japan Contacts No. 20025001, No. 20039001, and No. 20540251. The work of T. S. and O. V. was supported in part by MEC and FEDER (EC), Grants No. FPA2005-01678 and the Generalitat Valenciana for support under Grants No. PROMETEO/2008/004, No. GV05/267, and No. GVPRE/2008/003. The work of O. V. was also supported in part by European program MRTN-CT-2006-035482 Flavianet. The work of M. Y. was supported in part by the Grant-in-Aid for the Ministry of Education, Culture, Sports, Science, and Technology, Government of Japan (No. 20007555).

## APPENDIX: INTERACTION LAGRANGIAN

In this appendix, we give the relevant Lagrangian and the decay widths in the presence of LFV.

The slepton-neutralino-lepton interaction Lagrangian in neutralino mass eigenstate basis and sfermion flavor basis is

$$\begin{aligned} \mathcal{L}_{\tilde{f}-\tilde{\chi}^0-l} = & \sqrt{2}g_2 \sum_{i,\alpha} [(g_{i\alpha}^{LL}\tilde{f}_\alpha^* + g_{i\alpha}^{RL}\tilde{f}_{\alpha+3}^*)\tilde{\chi}_i^0 P_L l_\alpha \\ & + (g_{i\alpha}^{RR}\tilde{f}_{\alpha+3}^* + g_{i\alpha}^{LR}\tilde{f}_\alpha^*)\tilde{\chi}_i^0 P_R l_\alpha] + \text{H.c.} \end{aligned} \quad (\text{A1})$$

where  $\tilde{\chi}_i^0$  denote mass eigenstate neutralinos and  $i$  runs over 1 to 4, and  $\tilde{f}_\alpha = (\tilde{e}_L, \tilde{\mu}_L, \tilde{\tau}_L)$  and  $\tilde{f}_{\alpha+3} = (\tilde{e}_R, \tilde{\mu}_R, \tilde{\tau}_R)$  denote flavor sleptons and  $\alpha$  runs over 1 to 3.  $P_{L,R}$  are the chirality projection operators and  $g_2$  is the  $SU(2)$  coupling constant. The constants,  $g_{i\alpha}^{ab}$ , couple sleptons of chirality “ $a$ ” to leptons of chirality “ $b$ .”

$$\begin{aligned} g_{i\alpha}^{LL} &= -\eta_i^* [T_{3L}(N)_{i2} + (Q - T_{3L}) \tan\theta_W(N)_{i1}], \\ g_{i\alpha}^{RL} &= \eta_i^* \frac{m_{l_\alpha}}{m_W \cos\beta} (N)_{i3}, \\ g_{i\alpha}^{RR} &= \eta_i Q \tan\theta_W(N)_{i1}, \quad g_{i\alpha}^{LR} = \eta_i \frac{m_{l_\alpha}}{m_W \cos\beta} (N)_{i3}, \end{aligned} \quad (\text{A2})$$

where  $Q$  and  $T_{3L}$  are the electric charges and  $SU(2)$  charge of leptons, and  $\theta_W$  is the Weinberg angle.  $N_{ij}$  is the diagonalization matrix of the neutralino mass matrix.

The slepton mass matrix is diagonalized by a unitary matrix and the mass eigenstate sleptons,  $\tilde{l}_k$ , with masses are  $m_{\tilde{l}_k}$ , are expressed by

$$\tilde{l}_k = R_{k\alpha} \tilde{f}_\alpha. \quad (\text{A4})$$

We define  $R$  according to  $m_{\tilde{l}_k} > m_{\tilde{l}_{k'}}$  for  $k > k'$ . Then, the relevant interaction Lagrangian in the mass eigenstate basis is given by

$$\begin{aligned} \mathcal{L}_{\text{int}} = & \sqrt{2}g_2 \sum_{i=1}^4 \sum_{k=1}^6 \tilde{l}_k^* \tilde{\chi}_i^0 \sum_{\alpha=e,\mu,\tau} [g_{i\alpha k}^L P_L l_\alpha + g_{i\alpha k}^R P_R l_\alpha] \\ & + \frac{G_F}{\sqrt{2}} \sum_{\alpha=e,\mu,\tau} (\bar{\nu}_\alpha \gamma_\mu P_L l_\alpha) J^\mu \\ & + \frac{4G_F}{\sqrt{2}} \sum_{\alpha,\beta=e,\mu,\tau} (\bar{\nu}_\alpha \gamma_\mu l_\alpha) (\bar{\nu}_\beta \gamma_\mu l_\beta) + \text{H.c.} \end{aligned} \quad (\text{A5})$$

Here  $G_F$  is the Fermi coupling constant,  $J^\mu$  is the pion current, and  $g_{i\alpha k}^L, g_{i\alpha k}^R$  are

$$g_{i\alpha k}^L = g_{i\alpha}^{LL} R_{k\alpha} + g_{i\alpha}^{RL} R_{k\alpha+3}, \quad (\text{A6})$$

$$g_{i\alpha k}^R = g_{i\alpha}^{RR} R_{k\alpha+3} + g_{i\alpha}^{LR} R_{k\alpha}. \quad (\text{A7})$$

The expression of these coupling constants in MI approximation is given in Eqs. (12) and (13).

The decay widths can be obtained by replacing  $g_L$  and  $g_R$  in Ref. [2] with  $g_{1\alpha 1}^{L,R}$ . The two-body decay width,  $\tilde{l}_1 \rightarrow \tilde{\chi}_1^0 + l_\alpha$  where  $l_\alpha = (e, \mu)$ , is given by

$$\begin{aligned} \Gamma_{2\text{-body}} = & \frac{g_2^2}{8\pi m_{\tilde{l}_1}^3} (\delta m (\delta m + 2m_{\tilde{\chi}_1^0}) \{ \delta m (\delta m + 2m_{\tilde{\chi}_1^0}) \\ & - 2m_{l_\alpha}^2 \} + m_{l_\alpha}^4)^{1/2} \{ (|g_{1\alpha 1}^L|^2 + |g_{1\alpha 1}^R|^2) (\delta m (\delta m \\ & + 2m_{\tilde{\chi}_1^0}) - m_{l_\alpha}^2) - 4 \text{Re}[g_{1\alpha 1}^L g_{1\alpha 1}^{R*}] m_{l_\alpha} m_{\tilde{\chi}_1^0} \}. \end{aligned} \quad (\text{A8})$$

The three-body decay width,  $\tilde{l}_1 \rightarrow \tilde{\chi}_1^0 + \nu_{l_\alpha} + \pi$  where  $l_\alpha = (e, \mu, \tau)$ , is given by

$$\begin{aligned} \Gamma_{3\text{-body}} = & \frac{g_2^2 G_F^2 f_\pi^2 \cos^2\theta_c ((\delta m)^2 - m_\pi^2)}{8(2\pi)^3 m_{\tilde{l}_1}^3} \\ & \times \int_0^1 dx \sqrt{((\delta m)^2 - q_\pi^2)((\delta m + 2m_{\tilde{\chi}_1^0})^2 - q_\pi^2)} \\ & \times \frac{(q_\pi^2 - m_\pi^2)^2}{(q_\pi^2 - m_{l_\alpha}^2)^2 + (m_{l_\alpha} \Gamma_{l_\alpha})^2} \frac{1}{q_\pi^2} \left[ \frac{1}{4} (|g_{1\alpha 1}^L|^2 q_\pi^2 \right. \\ & + |g_{1\alpha 1}^R|^2 m_{l_\alpha}^2) ((\delta m)^2 + 2m_{\tilde{\chi}_1^0} \delta m - q_\pi^2) \\ & \left. - \text{Re}[g_{1\alpha 1}^L g_{1\alpha 1}^{R*}] m_{\tilde{\chi}_1^0} m_{l_\alpha} q_\pi^2 \right], \end{aligned} \quad (\text{A9})$$

where  $q_\pi^2 = (\delta m)^2 - ((\delta m)^2 - m_\pi^2)x$ , and  $\Gamma_l$  is the decay width of the charged lepton,  $l$  ( $\Gamma_e = 0$ ).  $\theta_c$  is the Cabbibo angle.

The four-body decay width,  $\tilde{l}_1 \rightarrow \tilde{\chi}_1^0 + \nu_{l_\alpha} + \nu_{l_\beta} + l_\beta$  where  $l_\alpha = (e, \mu, \tau)$  and  $l_\beta = (e, \mu)$ , is given by

$$\begin{aligned} \Gamma_{4\text{-body}} = & \frac{g_2^2 G_F^2 ((\delta m)^2 - m_{\tilde{l}_\beta}^2)}{12(2\pi)^5 m_{\tilde{l}_1}^3} \int_0^1 dx \sqrt{((\delta m)^2 - q_{l_\beta}^2)((\delta m + 2m_{\tilde{\chi}_1^0})^2 - q_{l_\beta}^2)} \frac{1}{(q_{l_\beta}^2 - m_{l_\alpha}^2)^2 + (m_{l_\alpha} \Gamma_{l_\alpha})^2} \frac{1}{q_{l_\beta}^4} \\ & \times \left[ \frac{1}{4} (|g_{1\alpha 1}^L|^2 q_{l_\beta}^2 + |g_{1\alpha 1}^R|^2 m_{l_\alpha}^2) ((\delta m)^2 + 2m_{\tilde{\chi}_1^0} \delta m - q_{l_\beta}^2) - \text{Re}[g_{1\alpha 1}^L g_{1\alpha 1}^{R*}] m_{\tilde{\chi}_1^0} m_{l_\alpha} q_{l_\beta}^2 \right] \\ & \times \left[ 12m_{l_\beta}^4 q_{l_\beta}^4 \log \left[ \frac{q_{l_\beta}^2}{m_{l_\beta}^2} \right] + (q_{l_\beta}^4 - m_{l_\beta}^4)(q_{l_\beta}^4 - 8m_{l_\beta}^2 q_{l_\beta}^2 + m_{l_\beta}^4) \right], \end{aligned} \quad (\text{A10})$$

where  $q_{l_\beta}^2 = (\delta m)^2 - ((\delta m)^2 - m_{l_\beta}^2)x$ .

- 
- [1] K. Griest and D. Seckel, Phys. Rev. D **43**, 3191 (1991).  
[2] T. Jittoh, J. Sato, T. Shimomura, and M. Yamanaka, Phys. Rev. D **73**, 055009 (2006).  
[3] T. Jittoh, K. Kohri, M. Koike, J. Sato, T. Shimomura, and M. Yamanaka, Phys. Rev. D **76**, 125023 (2007).  
[4] T. Jittoh, K. Kohri, M. Koike, J. Sato, T. Shimomura, and M. Yamanaka, Phys. Rev. D **78**, 055007 (2008).  
[5] S. G. Ryan, T. C. Beers, K. A. Olive, B. D. Fields, and J. E. Norris, Astrophys. J. **530**, L57 (2000).  
[6] R. H. Cyburt, B. D. Fields, and K. A. Olive, Phys. Lett. B **567**, 227 (2003).  
[7] A. Coc, E. Vangioni-Flam, P. Descouvemont, A. Adahchour, and C. Angulo, Astrophys. J. **600**, 544 (2004).  
[8] N. Jarosik *et al.* (WMAP Collaboration), Astrophys. J. Suppl. Ser. **170**, 263 (2007).  
[9] J. Dunkley *et al.* (WMAP Collaboration), arXiv:0803.0586.  
[10] For a review and further references, see: G. G. Ross, in *Prepared for Theoretical Advanced Study Institute in Elementary Particle Physics (TASI 2000): Flavor Physics for the Millennium, Boulder, Colorado, 4–30 June 2000*, edited by J. L. Rosner (World Scientific, Singapore, 2001), p. 871.  
[11] M. Raidal *et al.*, arXiv:0801.1826.  
[12] K. Agashe and M. Graesser, Phys. Rev. D **61**, 075008 (2000).  
[13] F. Deppisch, H. Pas, A. Redelbach, R. Ruckl, and Y. Shimizu, Phys. Rev. D **69**, 054014 (2004).  
[14] F. Deppisch, J. Kalinowski, H. Pas, A. Redelbach, and R. Ruckl, arXiv:hep-ph/0401243.  
[15] A. Bartl, K. Hidaka, K. Hohenwarter-Sodek, T. Kernreiter, W. Majerotto, and W. Porod, Eur. Phys. J. C **46**, 783 (2006).  
[16] A. Ibarra and S. Roy, J. High Energy Phys. 05 (2007) 059.  
[17] K. Hohenwarter-Sodek and T. Kernreiter, J. High Energy Phys. 06 (2007) 071.  
[18] M. Hirsch, J. W. F. Valle, W. Porod, J. C. Romao, and A. Villanova del Moral, Phys. Rev. D **78**, 013006 (2008).  
[19] M. Hirsch, S. Kaneko, and W. Porod, Phys. Rev. D **78**, 093004 (2008).  
[20] K. Hamaguchi, M. M. Nojiri, and A. de Roeck, J. High Energy Phys. 03 (2007) 046.  
[21] S. Tarem *et al.* (ATLAS Collaboration), Report No. ATL-SN-ATLAS-2008-071.  
[22] S. Tarem *et al.*, Report No. ATL-PHYS-PUB-2005-02.  
[23] K. Ishiwata, T. Ito, and T. Moroi, Phys. Lett. B **669**, 28 (2008).  
[24] W. Porod, Comput. Phys. Commun. **153**, 275 (2003).  
[25] G. Belanger, F. Boudjema, A. Pukhov, and A. Semenov, arXiv:0803.2360.  
[26] G. W. Bennett *et al.* (Muon G-2 Collaboration), Phys. Rev. D **73**, 072003 (2006).  
[27] M. Davier, Nucl. Phys. B, Proc. Suppl. **169**, 288 (2007).  
[28] J. R. Ellis, T. Falk, K. A. Olive, and M. Srednicki, Astropart. Phys. **13**, 181 (2000); **15**, 413(E) (2001).  
[29] An interesting question in the long-lived stau region is the possibility to detect a long-lived stau at neutrino telescopes through inelastic scattering of high-energy neutrinos. However, the expected number of events in our scenario is always small and the neutrino telescope will not put a strong constraint [30].  
[30] B. Cañadas, D. G. Cerdeño, C. Muñoz, and S. Panda (work in progress).  
[31] L. Calibbi, J. Jones-Perez, and O. Vives, Phys. Rev. D **78**, 075007 (2008).  
[32] I. Masina and C. A. Savoy, Nucl. Phys. **B661**, 365 (2003).  
[33] M. Ciuchini, A. Masiero, P. Paradisi, L. Silvestrini, S. K. Vempati, and O. Vives, Nucl. Phys. **B783**, 112 (2007).  
[34] F. Borzumati and A. Masiero, Phys. Rev. Lett. **57**, 961 (1986).  
[35] J. Hisano, T. Moroi, K. Tobe, M. Yamaguchi, and T. Yanagida, Phys. Lett. B **357**, 579 (1995).  
[36] J. Hisano and D. Nomura, Phys. Rev. D **59**, 116005 (1999).  
[37] J. Sato and K. Tobe, Phys. Rev. D **63**, 116010 (2001).  
[38] J. Sato, K. Tobe, and T. Yanagida, Phys. Lett. B **498**, 189 (2001).  
[39] J. A. Casas and A. Ibarra, Nucl. Phys. **B618**, 171 (2001).  
[40] S. Lavignac, I. Masina, and C. A. Savoy, Phys. Lett. B **520**, 269 (2001).  
[41] A. Kageyama, S. Kaneko, N. Shimoyama, and M. Tanimoto, Phys. Lett. B **527**, 206 (2002).  
[42] A. Kageyama, S. Kaneko, N. Shimoyama, and M. Tanimoto, Phys. Rev. D **65**, 096010 (2002).

- [43] A. Masiero, S.K. Vempati, and O. Vives, Nucl. Phys. **B649**, 189 (2003).
- [44] F. Deppisch, H. Pas, A. Redelbach, R. Ruckl, and Y. Shimizu, Eur. Phys. J. C **28**, 365 (2003).
- [45] A. Masiero, S.K. Vempati, and O. Vives, New J. Phys. **6**, 202 (2004).
- [46] T. Ota and J. Sato, Phys. Rev. D **71**, 096004 (2005).
- [47] S.T. Petcov, W. Rodejohann, T. Shindou, and Y. Takanishi, Nucl. Phys. **B739**, 208 (2006).
- [48] S. Antusch, E. Arganda, M.J. Herrero, and A. M. Teixeira, J. High Energy Phys. **11** (2006) 090.
- [49] G.G. Ross, L. Velasco-Sevilla, and O. Vives, Nucl. Phys. **B692**, 50 (2004).
- [50] S. Antusch, S.F. King, M. Malinsky, and G.G. Ross, arXiv:0807.5047.
- [51] F. Feruglio, C. Hagedorn, Y. Lin, and L. Merlo, arXiv:0807.3160.
- [52] R. Barbieri and L.J. Hall, Phys. Lett. B **338**, 212 (1994).
- [53] R. Barbieri, L.J. Hall, and A. Strumia, Nucl. Phys. **B445**, 219 (1995).
- [54] L. Calibbi, A. Faccia, A. Masiero, and S.K. Vempati, J. High Energy Phys. **07** (2007) 012.
- [55] L. Calibbi, Y. Mambrini, and S.K. Vempati, J. High Energy Phys. **09** (2007) 081.
- [56] S. Bentvelsen *et al.* (ATLAS Collaboration), JINST **3**, S08003 (2008).
- [57] For more information on the ATLAS Experiment, visit their website <http://atlas.ch/>.
- [58] R. Adolphi *et al.* (CMS Collaboration), JINST **3**, S08004 (2008).
- [59] M. Battaglia *et al.*, Eur. Phys. J. C **22**, 535 (2001).
- [60] M. Battaglia, A. De Roeck, J.R. Ellis, F. Gianotti, K. A. Olive, and L. Pape, Eur. Phys. J. C **33**, 273 (2004).
- [61] For different values of  $\tan\beta$ , branching ratios for each decay are different but the total branching ratio will be the same.
- [62] P.Z. Skands, Eur. Phys. J. C **23**, 173 (2002).
- [63] Taking into account that the production cross section is almost identical for different values of  $\tan\beta$ , we use the cross section for point  $P_2 \simeq J'$  in [62].
- [64] S. Kaneko, J. Sato, T. Shimomura, O. Vives, and M. Yamanaka (work in progress).